

Exchange between a freshwater embayment and a large lake through a long, shallow channel

Francisco J. Rueda¹ and Edwin A. Cowen²

Defrees Hydraulics Laboratory—School of Civil and Environmental Engineering, Cornell University, Ithaca, New York 14853

Abstract

We analyze the exchange between a weakly forced lacustrine embayment and a large lake through a long, shallow channel. Exchange in the channel is the result of a multiple and subtle balance in which spatial thermal variations (baroclinic forcing), oscillations in the water level (barotropic forcing), bottom friction, diffusion, wind forcing, and the effects of unsteadiness are all important. Temperature gradients across the channel result from differences in thermal inertia of the embayment and lake at seasonal time scales and differences in the wind-driven internal dynamics of the lake and the embayment at diurnal to synoptic time scales. These gradients are, in general, weak and barotropic forcing dominates the channel momentum balance; however, episodic upwelling in the lake can shift the balance in favor of baroclinic dominance. A combination of scaling, analysis of observational data, and three-dimensional simulations are used to demonstrate that bed stress, vertical turbulent diffusion, wind stress, and unsteadiness effect exchange relative to the predictions of internal hydraulic theory—the quasisteady inviscid theory that describes the motion resulting from a purely barotropic/baroclinic force balance.

The performance of aquatic systems, often characterized as biological and chemical reactors or chemostats, is, to a great extent, dependent on hydrodynamic processes. Hydrodynamic processes determine the environmental conditions that affect the biogeochemistry, and importantly, the length of time water and its constituents remain in the system. This time scale, generally known as the hydraulic residence time, has been proposed in the literature to explain a range of water-quality phenomena, such as the variability in lake eutrophication processes, thermal stratification, isotopic composition, alkalinity, dissolved organic carbon concentration, elemental ratios of heavy metals and nutrients, mineralization rates of organic matter, and primary production (see Monsen et al. 2002 for a list of references). The experiments of Fussman et al. (2000) go further, suggesting that residence time scales control the structure of aquatic ecosystems and the extent that these systems are self-organized or dominated by exogenous influences.

In semiencllosed basins separated by topographic constrictions (sills, contractions, or their combinations) from adjoining oceans, their residence time scale, and hence, their biogeochemical behavior are determined by the rate at which

oceanic water enters the basin and replaces basin water. The mass fluxes between the basin and ocean, known as the exchange, are in turn the result of transport processes acting on multiple spatial and temporal scales. Given the differences in the range and magnitude of forcing mechanisms and, hence, in the scales of the transport processes, one would expect differences between the exchange processes observed in lacustrine environments and those observed in large oceanic systems (such as the Bosphorus Strait or the Strait of Gibraltar) or in coastal lagoons. Most applications of the theoretical developments in exchange flows through topographic constrictions pertain to the fields of physical and coastal oceanography and little research on lake–embayment exchange has been published.

In this article, we analyze the exchange between a weakly forced lacustrine embayment and a large lake through a long, shallow channel, with particular emphasis on the component physical processes and their forcing mechanisms, that establish the net exchange. We use Little Sodus Bay (43°20'N, 76°42'30"W) as our field laboratory and canonical weakly forced system. Little Sodus Bay (LSB; Fig. 1) is a freshwater embayment with negligible through-flow but permanent connection to Lake Ontario (LO) through a shallow (2–3 m), narrow (75 m), and long (550 m) channel. It represents a common class of freshwater embayments existing along the boundaries of the Great Lakes and many other large lakes of the world. Transport in LSB is forced by variable and weak winds, spatial thermal variations, and oscillations in the water level, which, even in extreme cases, are at most on the order of 10 cm (discussed further in the “Results and discussion” section). Because the system (e.g., its stratification) changes on a seasonal basis, the analysis of the transport processes that drives exchange also needs to be done across seasonal time scales.

Finnigan and Ivey (1999), Finnigan and Ivey (2000), and Finnigan et al. (2001) have used a physical model coupled with numerical simulations to analyze the exchange and cir-

¹ Present address: Instituto del Agua, Universidad de Granada, 18071 Granada, Spain.

² Corresponding author (eac20@cornell.edu).

Acknowledgments

The authors thank all the researchers working in the Lake Ontario Biocomplexity Study—in particular, Gail Steinhart, Andrea Parmenter, Rebecca Doyle, and Stephen Monismith, Stanford University, for the loan of his two Sontek ADVs. We are indebted to staff and students in Defrees Hydraulic Laboratory at Cornell University, who assisted in the instrument deployment and retrieval—in particular, we thank Alexandra King, P. J. Rusello, Kristi Kull, and Aaron Blake. The authors acknowledge funding from the National Science Foundation: Biocomplexity in the Environment Program, OCE-0083625 and CTS-0093794, and the Office of Naval Research, N00014-98-1-0774.

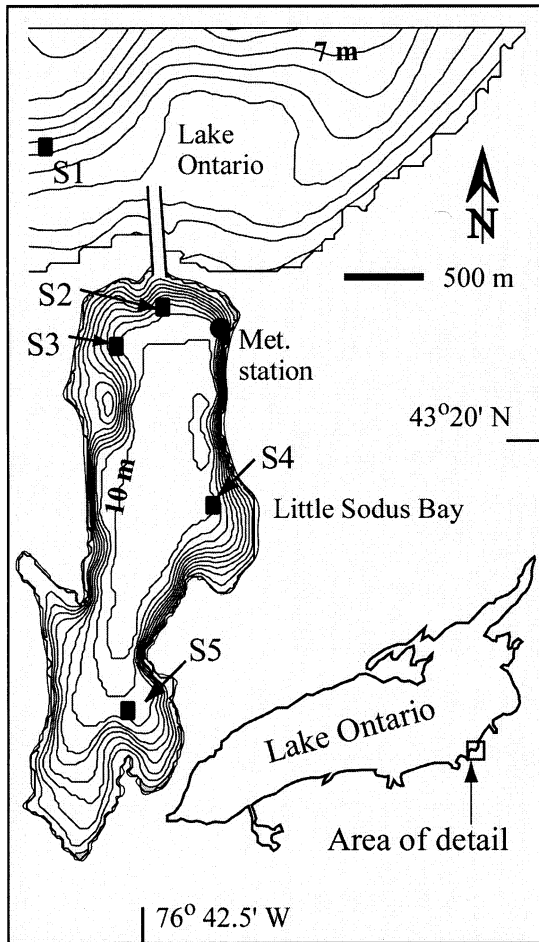


Fig. 1. Location and bathymetric map of Little Sodus Bay. Contours are shown every meter, and the 10-m and 7-m isobaths are shown in Little Sodus Bay and Lake Ontario, respectively. The bay is connected to the lake through a channel that is 550 m long, 75 m wide, and 3 m deep. Thermistor chain locations are shown as black squares and are identified as S1, S2, S3, S4, and S5.

ulation, in the absence of tidal forcing, in a basin of uniform depth and width separated from an ocean by a smooth sill. Fluid motion was exclusively driven by longitudinal gradients resulting from differential buoyancy fluxes on both sides of the sill. Their laboratory experiments and numerical simulations describe the adjustment of the basin circulation and exchange in response to steady and periodic buoyancy forcing until the circulation and exchange reach a steady state, characterized by a balance between inertia, buoyancy, and mixing processes. They determine appropriate scaling laws relating the energetics of the flow to external parameters, such as buoyancy fluxes and geometrical characteristics. This body of work is based on an elegant idealization of natural systems, such as LSB, and is an excellent starting point for investigating the complexities arising from the non-steady, and usually nonperiodic, effects of wind and buoyancy forcing, the earth's rotation, and the effects of natural and in general more complicated bathymetries. Given the complexities that result from multiple forcing mechanisms, we approach the problem of determining lake-embayment

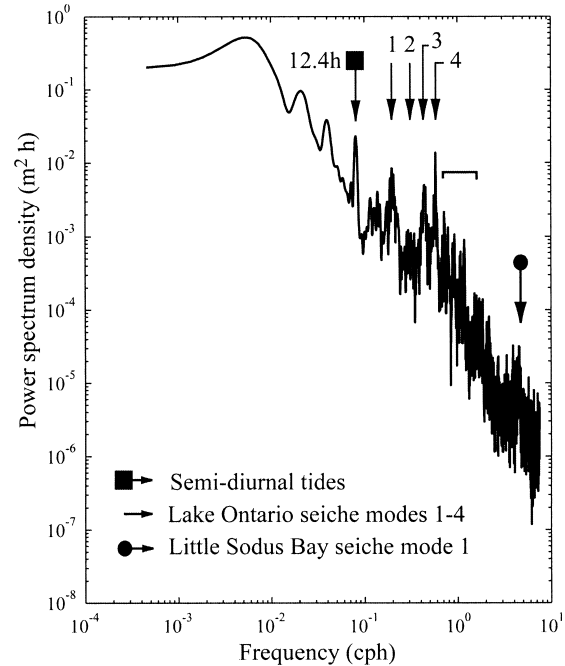


Fig. 2. Power spectral density of water-surface elevations in Little Sodus Bay, based on raw 2-min pressure records after detrending. The arrows mark the semidiurnal tides, the first four seiche modes in Lake Ontario (according to Hamblin 1982), and the first seiche mode of Little Sodus Bay.

exchange by analyzing a series of short-term field experiments to identify the important physical processes and establish their respective scales and ranges of variability. Time-resolved unsteady, three-dimensional numerical simulations are then conducted to further explore the physical processes themselves.

Little Sodus Bay: physical environment—Little Sodus Bay is a relatively small embayment on the south shore of Lake Ontario (Fig. 1). It has a small contributing watershed, from which it receives an annual mean daily discharge of approximately $0.15 \text{ m}^3 \text{ s}^{-1}$. The embayment has a surface area of 2.96 km^2 , a maximum depth of about 12 m, and a total volume of $2 \times 10^7 \text{ m}^3$. It is approximately 4 km long and 1 km wide, and it is connected to LO through a man-made channel with design length, width, and depth of 550, 75, and 3 m, respectively. At the mean level of LO, the water depth in the channel is approximately 2.4 m. LO water level undergoes oscillations on a wide range of time scales, including seasonal, synoptic (caused by weather phenomena, specifically wind), and subdiurnal. Oscillations with periods shorter than diurnal include the semidiurnal tides and seiches. The four lowest mode surface seiches have periods of 5.06, 3.21, 2.32, and 1.75 h (Hamblin 1982, and the surface displacement spectrum in Fig. 2). The strongest wind events affecting LSB are in general from the west-northwest (synoptic), while the embayment is subject most frequently to relatively weak northerly or southerly winds, most probably of a local nature (lake breezes). Westerly synoptic wind events drive increases in water levels along the southeastern shore of Lake Ontario (wind setup), while locally offshore winds (out

Table 1. Description of field experiments.

ID	Initial date	End date	Notes
E1	19 Oct 2001, day 290	3 Dec 2001, day 336	Temperature chains at S1, S2, S3, S4, S5—basin well mixed
E2	11 May 2002, day 130	29 May 2002, day 148	Temperature chains at S1, S2—pressure sensor in S2 (failed after 7 d)—temperature chain in channel on day 148—ADCP in channel failed
E3	8 Jun 2002, day 158	13 Jun 2002, day 163	Temperature chains at S1, S3, S4, S5—pressure sensor in S3 and S5—ADCP in the channel—ADCP boat mounted, only gives noisy data in transects across LSB
E4	13 Jul 2002, day 193	8 Sep 2002, day 250	Temperature chains at S1, S3, S4, S5—pressure sensor in S5; on July 19, ADCP and SCAMP were used for channel observations
E5	10 Oct 2002, day 282	11 Oct 2002, day 283	Temperature chains at S1 and S2; ADCP and ADV frame used for channel observations

of the south) drive more ephemeral drops in LO water level at LSB.

Materials and methods

Field experiments—To study lake–embayment exchange in LSB and its seasonal evolution, a series of experiments were conducted in 2001 and 2002 (Table 1). Water temperature (sampled every minute) is used here to trace water motions in areas where spatial gradients exist. Three to four thermistor strings, depending on the experiment (Table 1), equipped with Seabird SBE39 temperature and temperature–pressure loggers, were deployed in LSB at the locations shown in Fig. 1. An additional thermistor string (S1) was deployed in LO at distances of approximately 500–1,000 m west (depending on the experiment) of the entrance to LSB from LO along the 6-m isobath. The thermistors on each string were deployed with 1-m spacing beginning 0.5 m below the water surface.

Observations of the temperature and velocity field were also collected approximately at midchannel in the connection between LSB and LO during several hours in each of the 2002 experiments. In Experiment 2, three thermistors were deployed 0.5, 1.5, and 3 m below the water surface sampling at 1 Hz. An RDI-1200Khz Workhorse Monitor acoustic Doppler current profiler (ADCP) and a Nortek Vector acoustic Doppler velocimeter (ADV) were deployed at that same midchannel location in upward-looking orientations. The ADCP, however, generally failed to give valid velocity profiles due to the existence of strong exchange flow that induced vertical velocity shear in the water column. The velocity field was successfully monitored in Experiment 3 with the 1200-kHz ADCP programmed to record 5-s ensembles of 15 pings each in 10-cm bins in mode 5 (a pulse-to-pulse coherent mode). Midchannel temperature observations were not obtained in Experiment 3.

In Experiment 4, temperature microstructure and velocity observations were obtained using a Precision Measurement Engineering (PME) Self-Contained Autonomous Microstructure Profiler (SCAMP) and the RDI-1200Khz ADCP operating as in Experiment 3. In Experiment 5, and in an effort to further characterize turbulent stresses in the chan-

nel, a frame of three acoustic Doppler velocimeters (ADVs—two Sontek 10 MHz field ADVs and one Nortek Vector ADV) was deployed from 10 October 2002 until 11 October 2002, with the ADV measurement volumes located at elevations of 0.30, 1.50, and 2.50 m above the bed (flow depth was 3.0 m). The turbulent fluctuations were filtered from the wave-induced flows measured by the ADVs using a linear filtration and differencing technique to remove contamination by surface waves (Shaw and Trowbridge 2001). The technique is based on the analysis of two sensors spaced more than the integral length scale of the turbulence apart but considerably less than the surface-wave length apart. The filter was determined using all three components of the measured velocity and a filter weight length of 21 samples (corresponding to a 1.31-s filter for the 16-Hz sampled data), allowing the direct measurement of the Reynolds stresses and drag coefficients. The RDI 1200 kHz ADCP, operating in mode 11 with 5-cm bins and recording single-ping data at 6 Hz, was located in the vicinity of the ADV frame. The ADCP measured spectrum reveals the presence of moderate waves in the channel with period 3 s and amplitude of approximately 0.2 m during Experiment 5.

Wind speed and direction, solar radiation, relative humidity, and air temperature were monitored with a Campbell Scientific meteorological station located in the northeast end of LSB (Fig. 1). For Experiment 1, local atmospheric information is only available sporadically and data from Oswego are used (30 km east of LSB). Water level in Lake Ontario as measured in Oswego Harbor is also used in the analysis of data in Experiment 1. For the remainder of the experiments, local meteorological data were collected and water level fluctuations were measured with a Seabird SBE39 temperature–pressure logger located at Sta. S2.

Numerical simulations—The numerical simulations were conducted with the Princeton Ocean Model (POM; e.g., Blumberg and Mellor 1987). POM solves the three-dimensional Reynolds averaged Navier–Stokes equations, with the Boussinesq and hydrostatic approximations, and in sigma coordinates, using mode-splitting and explicit leapfrog algorithms. The computational domain (shown in Fig. 1) consists of the embayment, the connection, and a small part of

LO surrounding the connection (with a surface area of approximately 1 km^2). The domain has been discretized using cells of $25 \text{ m} \times 25 \text{ m}$ in the horizontal direction. A total of 24 layers are used for the vertical discretization, which gives a resolution of approximately 10 cm in the 2.4-m -deep lake–embayment connection. The model is forced at the open boundaries with water-level oscillations of 2 cm amplitude and 2 h period and by setting a fixed temperature at the boundary that differs by an amount ΔT_c from the uniform initial conditions in LSB (25°C). Three scenarios are investigated. In scenario 1 (typical conditions), the fixed temperature of LO is 23°C (i.e., ΔT_c 2°C); in scenario 2 (upwelling events), it is 6°C (ΔT_c 19°C); while in scenario 3 (wind), a moderate wind stress is added to the upwelling scenario. Clamped boundary conditions are used for water surface elevations and oblique radiation boundary conditions are used for all other hydrodynamic variables. The roughness length z_0 at the bottom of the domain is uniform and set to 1 cm . The model is run for 3 d, and only the last 20 cycles are used in the analysis.

Results and discussion

Cooling period—During fall, the embayment was well mixed, and the only source of inhomogeneity was the connection with LO. The temperature differences across the channel changed sign several times during this experiment, and in general, were weak, reaching a maximum of approximately 1°C . The temperature records from the shallowest thermistors at S1, S2, and S3, together with the time series of water levels in LO, are shown in Fig. 3a. This corresponds to a period when water in the lake is warmer than in the embayment. Water at S2 is a mixture of lake and embayment water, having a temperature intermediate between that at S3 and S1. The amount of lake water appearing at S2 strongly depends on the magnitude of the lake-level oscillations. On day 296, lake-level oscillations are weak, and the temperature at S2 is closer to that of the embayment. On day 297, a sequence of strong westerly winds (not shown) caused changes in lake levels of up to $10\text{--}12 \text{ cm}$, and Sta. S2 sees pulses of water with a significant portion of lake water coinciding with water level rises (note that there is clearly significant mixing, as the water temperature at S2 becomes at most approximately 70% LO water). Also the stratification at S2 is controlled by the magnitude of the barotropic oscillations (see Fig. 3b). On day 296, with weak barotropic forcing, the water column is stratified and only its shallower portion shows evidence of warmer water, a mixture of lake and embayment water. Under strong forcing, warmer lake water is the dominant component at all depths at S2 (see event at noon on day 297).

Warming period—During spring, water temperatures in the embayment increase faster than in LO due to differences in bathymetry, hence, in thermal inertia (differential heating). Experiments 2 and 3 were conducted during this period, though only the results of Experiment 2 will be presented and discussed. It was during Experiment 2 that both stations S2 and S1, in the near vicinity of the channel, were deployed.

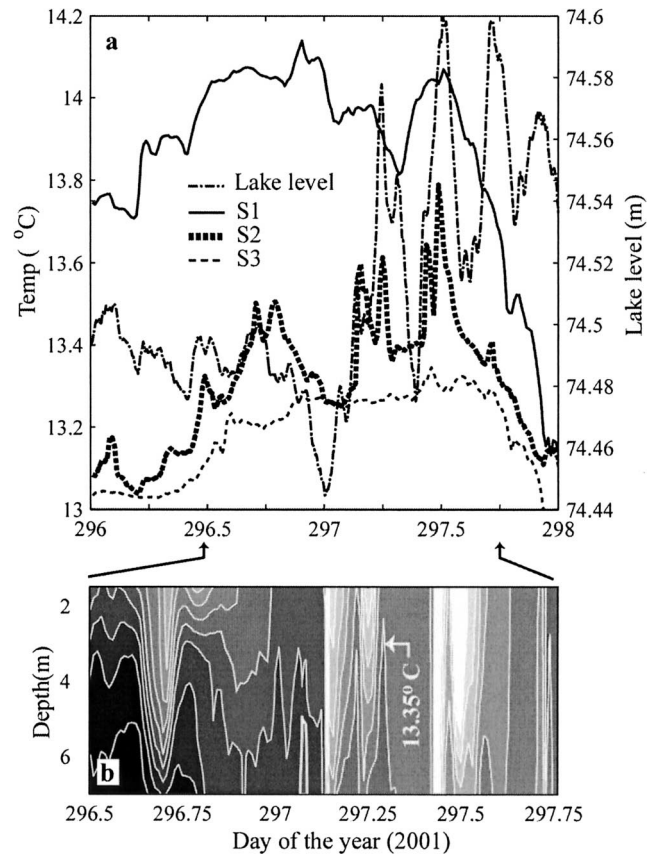


Fig. 3. (a) Time series of shallowest thermistor temperature at S1, S2, and S3 (left axis) for days 296–298, 2001, together with time series of lake level measured at Oswego Harbor (right axis). On day 297, westerly winds of up to 9 m s^{-1} blew over Lake Ontario, after a period of calm. (b) Time series of isotherm depths in Sta. S2 for 30 h starting noon on day 296. Isotherms are shown every 0.05°C , and the 13.35°C isotherm is labeled for reference. Records are shown every 15 min.

The magnitude of the lake-level oscillations around their mean values, and hence the energy of the barotropic forcing, varies over the experiment (Fig. 4a,b): the largest oscillations (of up to $4\text{--}6 \text{ cm}$) were observed from day 130 to 135 and also from day 143 to 146. During the rest of the observation period, only weak oscillations of up to $1\text{--}2 \text{ cm}$ were observed. Temperature differences across the channel measured at 1.5 m below the surface also vary, but for most of the experiment, are between 1°C and 3°C , and only on day 148, toward the end of the experiment, become large, reaching up to 6°C (Fig. 4b). With temperature differences of up to 3°C (until day 146), the lower thermistors at S2 only see colder lake water in short-lived pulses coincident with, or shortly after, flood events (southerly directed flows into LSB) and during periods of strong barotropic oscillations (Fig. 4a). These pulses of cold water are especially noticeable, for example, in the records of days 131 and 132. Because the deepest point at S2 is 4 m below the bottom of the channel, the occurrence of cold water pulses is indicative of selective withdrawal processes, in which colder lake water flows upward along the embayment bed during ebb periods (north-

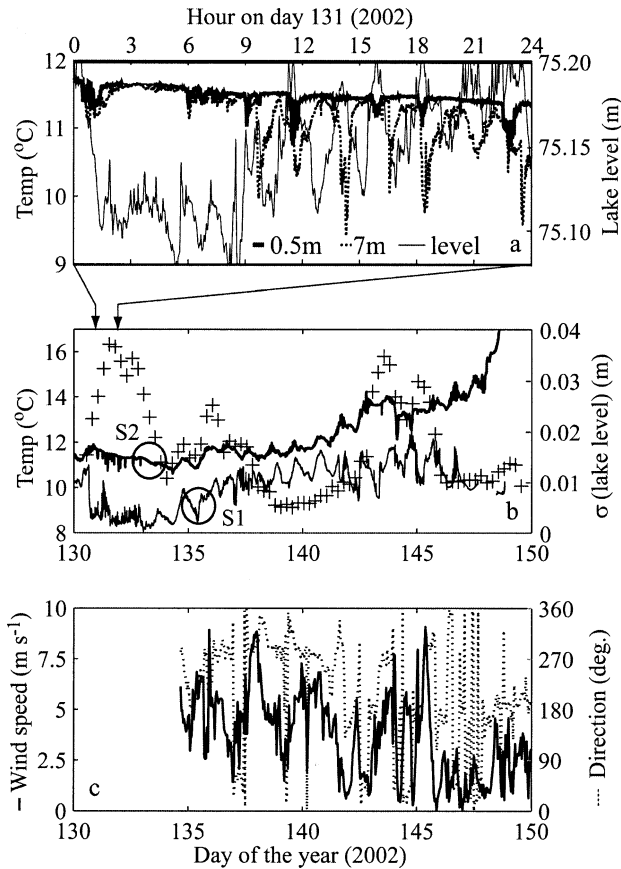


Fig. 4. (a) Time series of water temperature at 0.5 m (black dashed) and 7 m (black solid) below the free surface, and lake levels, all measured at S2, on day 131. (b) Time series of water temperatures at 1.5 m below the surface at S1 and S2, together with the standard deviation of Oswego Harbor water level records (local level records only span first 7 d of the experiment). The standard deviation is calculated on 24-h windows. (c) Wind records measured in Little Sodus Bay (data missing for the first 4 d of the experiment).

erly directed flows into LO). The 6°C temperature differences occur after a period of 2 d (146–147) of low wind when heat accumulates in the surface layer of LSB (Fig. 4c). On day 148, southerly winds blow over the embayment, raising the temperatures at S2 at all depths. On day 148, the lower thermistor at S2 (2 m above the bottom) detects colder lake water not in pulses, but over sustained periods of time, indicating that lake water is flowing more continuously into the embayment, likely a result of the coupled barotropic circulation and the baroclinic response to the export of the warm surface water out the channel surface layer.

The ADV and temperature observations collected on day 148 in the channel confirm that the lake water is indeed able to flow almost continuously into the embayment (see Fig. 5). The top and bottom thermistors in the channel reveal temperature differences of up to 6°C , equal to the temperature variation across the channel, which suggests that water flows in opposite directions at the top and bottom of the water column, i.e., a two-layer exchange flow pattern. The RDI-1200Khz ADCP (mode 11) generally failed to record valid data (most probably due to high shear in the water

column acting over relatively large, 25-cm, bins), but during the isolated periods when it recorded valid velocity data, it revealed changes in water velocity of approximately 15 cm s^{-1} over approximately 75 cm of the water column with a southerly directed flow at the bottom (i.e., into LSB) and a northerly directed flow at the surface (i.e., into LO). The temperature at 1.5 m decreases in response to rises in the water level and increases during ebb, revealing that the barotropic oscillations also modify the baroclinically driven exchange flow, moving the interface of an idealized two-layer system up and down.

The temperature measured 5 m below the free surface at S2 is $\sim 3\text{--}4^{\circ}\text{C}$ above the cold water observed at the bottom of the channel (10°C) and intermediate between lake and embayment temperatures, revealing the intense mixing that occurs as lake water enters the embayment as an underflow. Comparing the records at S2 and at the center of the channel, they do not seem to be correlated in time, indicating that the density gradient is sufficiently strong to avoid the withdrawal of cold water by the barotropically driven velocities in the channel during ebb flows.

Summer conditions—Temperature gradients across the channel: Temperature differences across the channel are in general weak during late summer, ranging from 0°C to $2\text{--}3^{\circ}\text{C}$ (Fig. 6a). Episodic winds with strong along-shore (easterly) component or offshore (southerly) component acting during the stratified season, either on a motionless basin or in phase with basin-scale Kelvin internal waves (see Antenucci et al. 2000; Rueda et al. 2003 for examples in medium-size lakes), can induce upwelling of hypolimnetic water along the south shore of LO, causing the temperature gradients across the channel to increase dramatically. The three dips in the lake temperature records shown in Fig. 6 correspond to a sequence of upwelling-favorable (according to the first-order model of Csanady 1977) northeasterly wind events on days 235, 240, and 244 (marked on Fig. 6b). Temperature differences across the channel on these days reached 16°C , which agrees with a typical summer temperature difference between the epilimnetic and hypolimnetic waters in LO (Schwab 1977). As suggested by the channel observations in Experiment 2, these along-channel temperature gradients could have driven water mass exchange in the channel, with cold lake water flowing continuously into the embayment along the bottom and warmer embayment water flowing out toward the lake along the surface. Temperature records at all three stations in LSB reveal the intrusion of cold lake water masses, which fill the bottom of the embayment (Fig. 6c for records in Sta. S4). Such compelling evidence of deep penetration of lake water in the embayment does not exist in any of the other three experiments nor during the majority of Experiment 4, when the influence of LO on LSB is restricted to the region close to the channel. These observations suggest that, during lake upwelling events, the strength of the baroclinic forcing is such that it becomes the dominant mechanism of circulation, both across the connection and, more importantly, within the embayment. During these events, the whole basin of LSB participates in the exchange of mass with LO. The analysis of historical wind records in Lake Ontario (data from buoys

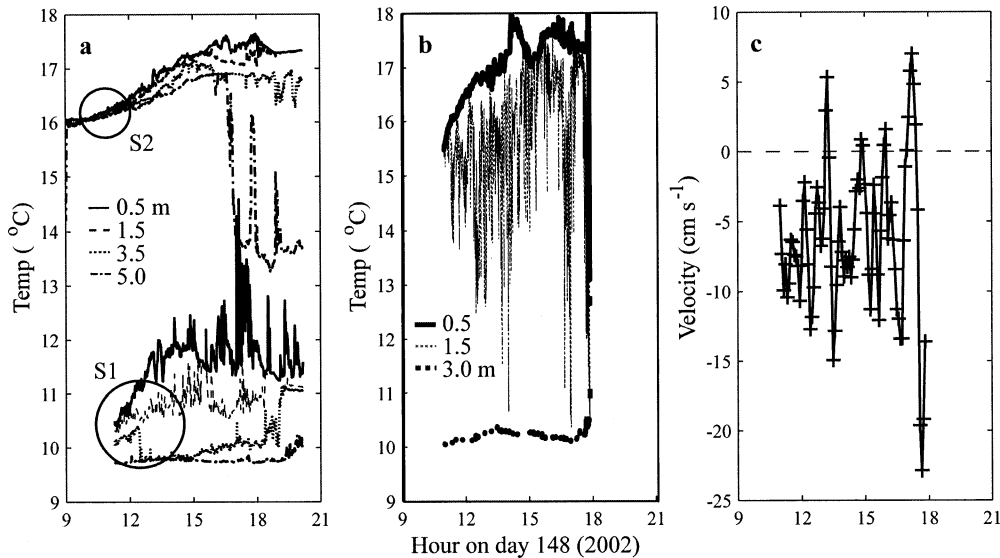


Fig. 5. Time series of (a) temperature at different depths at Sta. S1 and S2, (b) temperature at 3 depths at the channel, and (c) velocity at the bottom of the permanent connection between Little Sodus Bay and Lake Ontario (negative is flood, i.e., toward LSB).

45,139 and 45,135, in the north and western ends of the lake, respectively, and operated by Environment Canada) in the framework of the first-order thermocline-tilting model of Csanady (1977), suggests that upwelling events along southern LO, although episodic in nature, are not uncommon. These upwelling events lead to significant embayment–lake exchange events that may be critically important to the biology and ecology of an embayment.

Channel stratification under weak temperature gradients—On day 199, 2002, the difference in water temperature ΔT_c between LSB and LO is approximately 1°C and the water column is well mixed over the first 3–4 m (not shown). Under these conditions of weak ΔT_c , water in the channel moves back and forth from the lake to the embayment with almost no vertical velocity shear (see Fig. 7a), forced by the barotropic seiching motion in LO. The period of the oscillations is $T \sim 1\text{--}2$ h (the fourth mode seiche of LO from Fig. 2) and their amplitude U_0 is ~ 20 cm s⁻¹.

As revealed by the observed sequence of temperature profiles collected with a microstructure profiler (Fig. 7b), stratification is weak but persists during one oscillation cycle. Its evolution during one cycle shows parallelism with estuarine processes. First, the strength of the stratification varies within one cycle, being stronger in the transition from flood to ebb. Profile 2, for example, shows a sharp gradient at 1.5 m and was collected when barotropic forcing is minimal and the baroclinic forcing dominates the momentum balance, bringing colder lake water along the bottom of the profile. Also, stratification is stronger during ebb flows (profile 7) than during flood flows (profile 1), a feature that, in estuarine science, is known as strain-induced periodic stratification. A condition for the occurrence of this phenomenon is that the average stratification input over the ebb half of the oscillation cycle be greater than the mean tidal stirring power over

the same period (e.g., Simpson et al. 1990), which can be expressed as

$$\frac{1}{\rho} \frac{\partial \rho}{\partial x} > 2.2 \times 10^{-5} \left(\frac{U_0}{h} \right)^2 \quad (1)$$

where h is the depth of the water column. In the LSB channel on day 199, 2002, $1/\rho \partial \rho / \partial x \sim 5 \times 10^{-7}$ and $(U_0/h)^2 \sim 7 \times 10^{-3}$, and condition (1) is satisfied.

Stratification not only influences the mean velocity field (shear and exchange flow develop during ebb-flood transitions) but it can also affect turbulence in the water column, as shown by the analysis of the microstructure data. Figure 7c shows the $Re_T - Fr_T$ (activity) diagram that Ivey and Imberger (1991) use to define the state of turbulence. The turbulence Reynolds (Re_T) and Froude (Fr_T) numbers are calculated from estimates (derived from microstructure measurements) of the centered displacement scale L_c (a measure of the scale of the observed overturns), the Ozmidov length scale, L_o , and the Kolmogorov length scale, L_k as

$$Fr_T = \left(\frac{L_o}{L_c} \right)^{2/3} \quad \text{and} \quad Re_T = \left(\frac{L_c}{L_k} \right)^{4/3} \quad (2)$$

The range of turbulent Reynolds numbers observed in the channel data set ($10\text{--}10^4$) agrees with other field data compiled by Imberger and Ivey (1991) for lakes. The turbulent Froude numbers are mostly smaller than one, which suggests that the potential energy of the motions is predominantly balanced by the kinetic energy fluctuations. According to Luketina and Imberger (1989), region I in the activity diagram is characterized by isotropic turbulence, only mildly affected by stratification. Turbulence in region II is influenced considerably by stratification and, hence, is more anisotropic. Finally, in region III, only internal waves remain and the buoyancy flux is negligible. Our data set falls largely

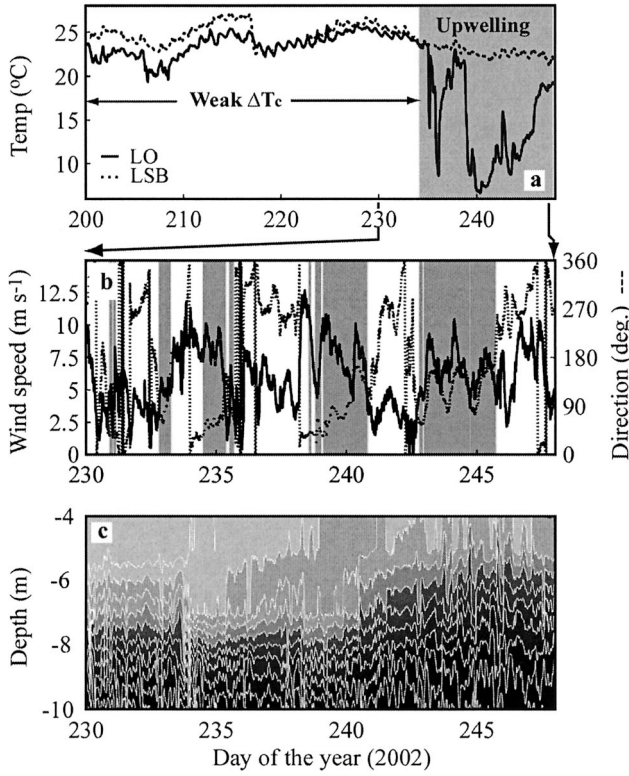


Fig. 6. Observations during Experiment 4 in 2002. (a) Time series of temperature 0.5 m below the surface in Lake Ontario and Little Sodus Bay. Two periods are marked, one with weak baroclinic forcing and a second with strong temperature differences between LSB and LO (upwelling). (b) Wind records for days 230–248, 2002, marking (in gray) those events favoring upwelling along the southeastern shore of LO. Data from NOAA buoy 45012 (<http://www.ndbc.noaa.gov>), located at the center of Lake Ontario. (c) Time series of temperature profiles (isotherms shown every 1°C) measured at Sta. S4. It shows the rising of isotherms that mark the deep penetration of LO waters in LSB.

along the boundary between regions II and III, which suggests that turbulence is indeed affected by the stratification.

Nature of exchange processes in the channel through scaling analysis: Barotropic and baroclinic forcings: The observational data reveal that, independent of season, the character of lake–embayment exchange is determined by two variables: the density differences between LO and LSB and the amplitude of the barotropic velocity oscillations in the channel, U_0 (or equivalently, the amplitude of the water level oscillations). It follows from dimensional arguments that these two variables can be grouped in a nondimensional number

$$F_0^2 = \frac{U_0^2}{g'H}, \quad \text{the internal Froude number} \quad (3)$$

Here, H is the depth of the channel, and g' is the reduced gravity. The internal Froude number defines the ratio of inertial to buoyancy forces, which, in internal hydraulic theory, are presumed to be the dominant terms in the momentum balance. Under barotropic forcing and using a quasisteady

approximation, in which the steady solutions apply at each point of the forcing cycle, internal hydraulic theory distinguishes between three exchange regimes (strong, intermediate, and moderate) according to the magnitude of F_0 (Armi and Farmer 1986; Farmer and Armi 1986). In the moderate regime, two layers of different density flow in opposite directions through the channel at all phases of the tidal cycle. The barotropic forcing in the other two regimes is sufficiently strong during maximum flood/ebb to arrest the flow in one of the layers (intermediate regime) and can even displace it from the channel and its immediate vicinity (strong regime, $F_0^2 > 1$). Pure two-layer exchange flows only exist when barotropic forcing is weak at slack tide. The distance to which the layer is displaced from the channel at maximum flood/ebb is also a function of F_0^2 and the particular geometry of the connection.

The lake–embayment exchange on day 297, 2001 (Experiment 1) occurs in the strong regime: estimated large U_0 of up to 50 cm s^{-1} coupled with weak temperature differences, ΔT_c , of at most 1°C lead to $F_0^2 \sim 50 > 1$. Hence, barotropic forcing dominates the exchange processes in the channel. Also, given the magnitude of F_0^2 , during flood periods, colder embayment water is displaced away from the channel into the basin and is even completely replaced by warmer lake water (see Fig. 3b). On day 199, 2002 (experiment 4), exchange occurs again in the strong regime with $F_0^2 \sim 5$, with velocity magnitudes typical of weak lake-level changes ($U_0 \sim 20 \text{ cm s}^{-1}$), and again very weak density gradients ($g' \sim 0.0025 \text{ m s}^{-2}$). Assuming a typical velocity scale $U_0 \sim 10\text{--}20 \text{ cm s}^{-1}$ in the channel, g' needs to be larger than $\sim 0.004\text{--}0.01 \text{ m s}^{-2}$ for the buoyancy forces to play an active role in the exchange process, i.e., $F_0^2 \sim 1$. Such conditions occur, for example, at the end of Experiment 2 when g' reaches ~ 0.009 .

Diffusive/hydraulic nature of the exchange flows: Exchange can occur either as a diffusive process, characterized by longitudinal density gradients and weak vertical stratification in the channel (Fig. 7a,b,c), or as an advective process, in which two distinct layers of different density flow in opposite directions through the channel (Fig. 5a,b,c), and therefore in any other mode between these two limiting cases. A parameter that defines the diffusive/hydraulic nature of the exchange flow in a given channel can be found by taking the square of the ratio of the vertical diffusive time scale to the time it takes a long-internal wave to propagate across the channel, which can be recast as the product of the Grashof number (Gr_T) and the square of the aspect ratio ($A = H/L$; Ivey 2004)

$$Gr_T A^2 = \frac{g'H^3}{K_v} \left(\frac{H}{L}\right)^2 \quad (4)$$

where K_v is the vertical eddy viscosity. If the exchange is diffusive, mixing balances buoyancy forces in the momentum equation, and all other terms (including inertia) can be neglected in the analysis (e.g., Officer 1976; Burling et al. 1999). In the internal hydraulic limit (e.g., Farmer and Armi 1986), buoyancy and inertia become the dominant terms in

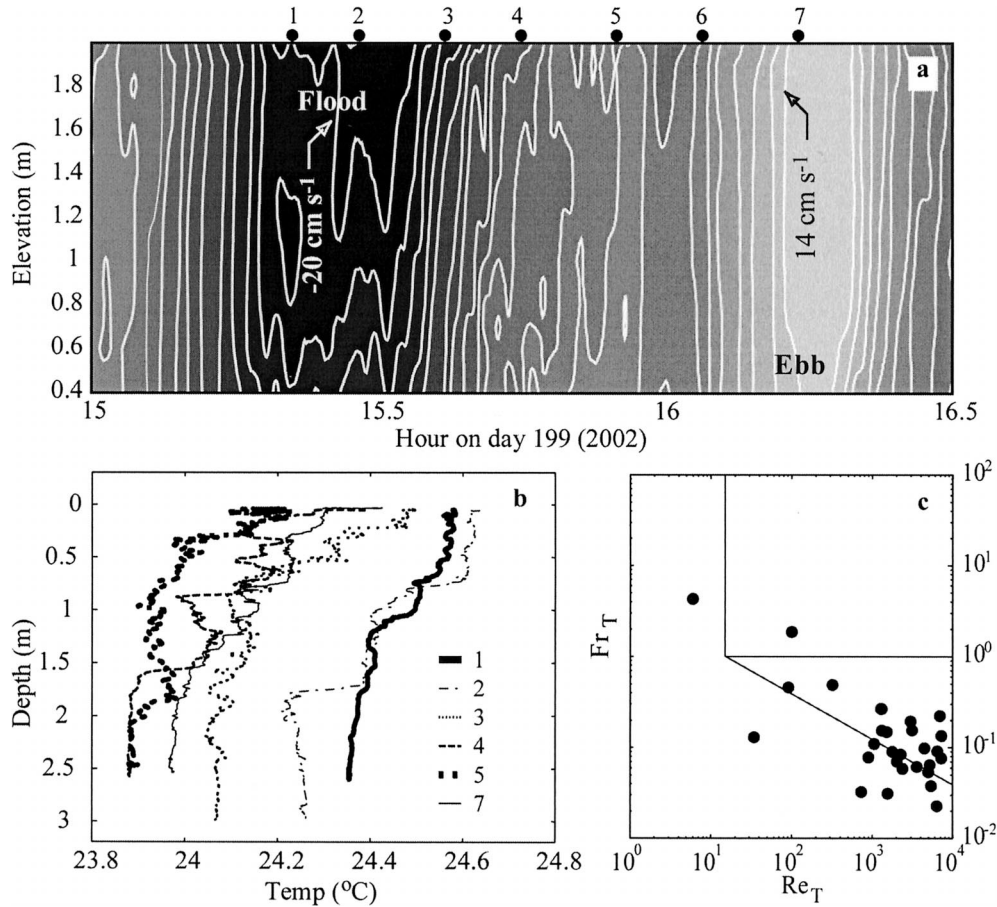


Fig. 7. Observation of channel processes during Experiment 4 in 2002. (a) Time series of longitudinal channel velocity profiles during 1½ h at the beginning of Experiment 4. Isotachs are shown every 2 cm s⁻¹ (-20 cm s⁻¹ and 14 cm s⁻¹ isotachs are given in the plot), time is represented along the x-axis and elevation from the bottom on the y-axis. The dots on the top of the figure mark times when temperature profiles were taken, and they are further identified with numbers. (b) Series of temperature profiles taken with SCAMP on day 199, 2002, at the center of the channel. The numbers indicate time when profiles were taken and are marked in panel a. (c) Fr_T - Re_T diagram for all microstructure profiles taken in the channel and marked in panel a.

the momentum balance, and friction (mixing) only induces secondary effects in the exchange.

The vertical eddy viscosity can be estimated from the ADV frame data collected during Experiment 5 as

$$K_v = -\frac{\overline{v'w'}}{\partial\bar{v}/\partial z} \quad (5)$$

Here, the along-channel vertical component of the turbulent stress (numerator) is determined from the Shaw and Trowbridge (2001) filtered data, and a central difference approximation is used to estimate of the mean along-channel velocity gradient (denominator). The results are shown in Fig. 8. Data with both low mean velocity gradient and low calculated Reynolds stress have been removed as the vertical homogeneity of the momentum field is not due to turbulent mixing. The values agree well with other estimates derived from microstructure measurements (not shown), which yield eddy diffusivities K_v in the range of $O(10^{-3}) < K_v < O(10^{-7})$ m² s⁻¹ (assuming a turbulent Prandtl number of one). Also

shown in Fig. 8 are the values of g' measured at each end of the channel based on the difference in temperature between 0.2 and 3 m below the surface. The values of $Gr_T A^2$ obtained based on the estimates of K_v range between order 1 and order 10⁸, lying either in the diffusive regime or in the transitional regime between the diffusive and internal hydraulic (advective) limits (Ivey 2004). This indicates that, although diffusive fluxes tend to dominate, the influence of the advective components cannot be ignored.

The importance of friction: The ratio of friction to inertial terms is (e.g., Gregg 2004),

$$\frac{C_d U^2}{h_2} \bigg/ \frac{U^2}{L} = \frac{C_d L}{h_2} \quad (6)$$

where h_2 , the lower layer depth, is taken to be approximately half of the channel depth and C_d is the bottom drag coefficient. Bottom friction should be important in long, shallow straits but not in short, deep straits. Based on Experiment 5

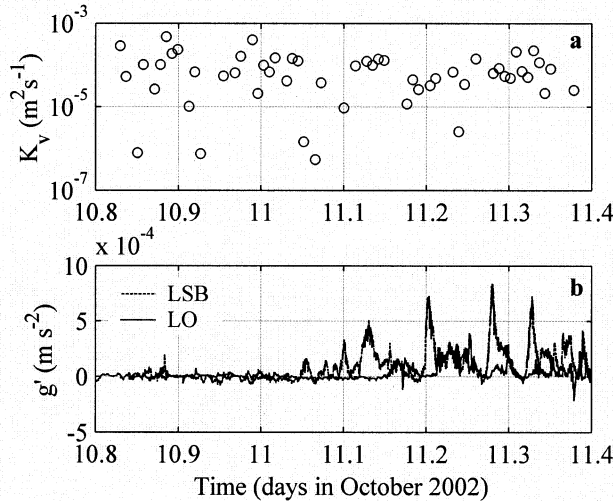


Fig. 8. (a) K_v estimated from ADV frame data and (b) g' estimated from the 0.2-m- and 3-m-deep thermistors located at the LO and LSB ends of the channel in Experiment 5.

data, the importance of friction can be estimated using Equation 6 and assuming $L \sim 500$ m—the length of the channel—and $h_2 \sim 1.5$ m—half the depth of the water column. The value of C_d is directly estimated from the lower two ADVs on the deployed ADV frame as

$$C_d = -\frac{\overline{v'w'}}{v^2} \quad (7)$$

where the root mean square velocity is used as the reference velocity scale due to the oscillatory nature of the flow (e.g., Cowen et al. 2003). The results, shown in Fig. 9, clearly suggest that bottom friction is often important throughout the tidal cycle.

Effects of unsteadiness: Helfrich (1995) established that, if the time for long internal waves to propagate through a channel, $\tau_w/(g'H)^{1/2}$, is the order of the time scale of the barotropic flow (the period of the oscillations, $T = 1\text{--}2$ h for LSB, based on our observations), unsteady effects cannot be neglected in the examination of exchange processes through the channel (i.e., the quasisteady analysis of Farmer and Armi (1986) is not valid). During Experiment 5, g' ranged between 1×10^{-4} and 8×10^{-4} m s^{-2} , yielding $\tau_w = 3\text{--}8$ h. Under stronger, but still mild stratifications, $\Delta T_c = 2^\circ\text{C}$, $\tau_w = 1$ h and, under strongly stratified (upwelling) conditions, $\Delta T_c \sim 10^\circ\text{C}$ and $\tau_w \sim 0.6$ h. Hence, unsteadiness cannot be ignored in the LSB–LO channel.

Numerical simulations—The observational and scaling analyses demonstrate that the channel connecting LSB and LO is highly unsteady, and friction and vertical turbulent mixing induced fluxes cannot, in general, be ignored. Based on this analysis, a numerical model has been used to explore the details of the exchange flows in the LSB channel. In Table 2, three fundamental scenarios are listed that were used to explore the exchange flow physics. The first, labeled typical, is based on typical conditions with weak along-channel temperature gradients relative to the magnitude of the

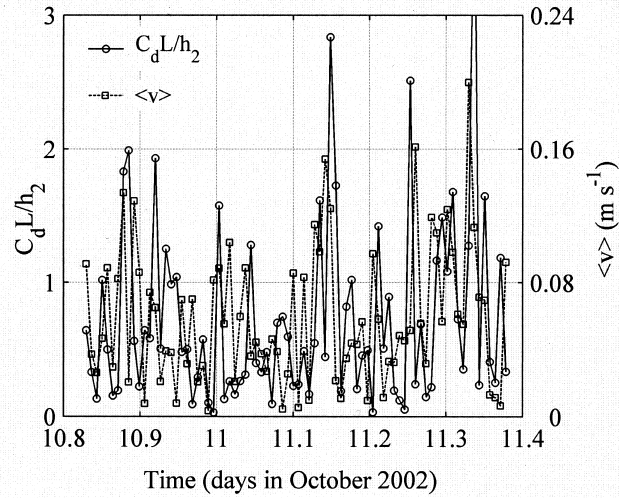


Fig. 9. Equation 6 value during Experiment 5 along with the mean magnitude of the along-channel velocity 0.3 m above the bed.

velocity oscillations, and the exchange is barotropically dominated ($F_0^2 > 1$). The second, labeled upwelling, is based on upwelling events in LO when the temperature difference across the channel can reach up to $15\text{--}20^\circ\text{C}$ (e.g., Fig. 6a) and buoyancy forces play a significant role in the determination of the exchange processes ($F_0^2 < 1$). In addition to the first two scenarios, in which barotropic and baroclinic forcing are the respective dominant processes, we analyze a third scenario, labeled wind, in which wind forces the exchange through the channel. Wind over LSB is predominantly from the southwest, although the most energetic events are either westerlies or northeasterlies. We only consider here the effects of southerly winds, which have mean values of $\sim 2\text{--}4$ m s^{-1} during the summer period. The consideration of wind forcing has not yet, to our knowledge, been incorporated in theoretical analysis of exchange flows through natural constrictions.

The results are presented as time series at the center of the channel and longitudinal sections along the center of the channel for both temperature and north–south velocities. The results shown in the longitudinal sections are phase averaged, with phase equal to zero when the water level reaches a maximum at the LO boundaries. The simulations are examined within the framework of two-layer internal hydraulic theory, using the midisotherm $\Delta T_c/2$ to separate the two layers in the continuous hydrodynamic field. In this theory, hydraulic controls in two-layer exchange flows occur at locations where the composite Froude number G^2 , defined as

Table 2. Conditions for the three numerically analyzed scenarios: typical, upwelling and wind.

	ΔT_c ($^\circ\text{C}$)	g' (m s^{-2})	U_0 (m s^{-1})	F_0^2	U_A (m s^{-1})
Typical	1–3	0.005	0.20	2.75	0
Upwelling	19	0.028	0.20	0.50	0
Wind	19	0.028	0.20	0.50	4 N

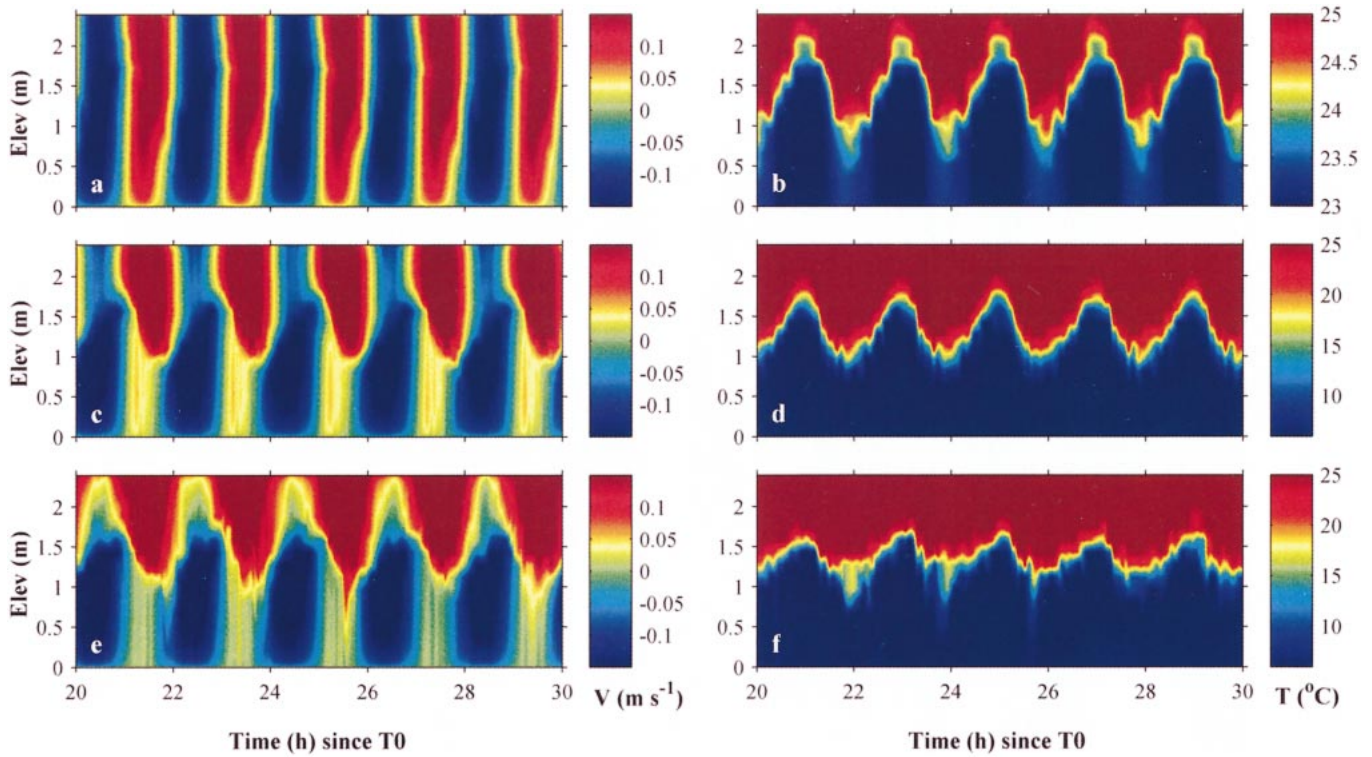


Fig. 10. Time series of longitudinal velocity (left column) and temperature (right column) profiles at the center of the channel for the three scenarios listed in Table 2: scenario 1 (a–b), scenario 2 (c–d), scenario 3 (e–f). T_0 represents the beginning of simulations.

$$G^2 = F_1^2 + F_2^2, \quad F_i^2 = \frac{u_i^2}{g'h_i} \quad (8)$$

is equal to one (Armi and Farmer 1986). Here, u_i is the (assumed uniform) speed of layer i , h_i is its thickness, and F_i^2 is the internal Froude number for layer i ($i = 1$ for surface layer). Two-layer exchange flow is subcritical when $G^2 < 1$ and supercritical when $G^2 > 1$. Maximal exchange flow through a channel with constant width and flat bottom, such as the LO–LSB connection, will have exit controls and subcritical flow in between (e.g., Assaf and Hecht 1974).

Under typical conditions (scenario 1), the water column oscillates back and forth in the channel from the LO to the LSB end with very little shear (indicative of a friction–buoyancy dominated exchange flow), and only during approximately 10% of the tidal cycle, toward the end of the ebb period, exchange flows develop at the center of the channel (Fig. 10a). Exchange flow also occurs at the channel center in the transition from flood to ebb, but it is very weak and short lived. The velocity field is therefore effectively dominated by barotropic forcing. Water from LO (23°C) or LSB (25°C) is never completely removed from the center section of the channel (Fig. 10b). As shown in Fig. 11a, a wedge is established in the channel and moves back and forth from the LSB end to the LO end of the channel within one tidal cycle. This feature appears in the intermediate regime defined in Armi and Farmer (1986), although it occurs here for much higher values of F_0^2 (~ 3). In the intermediate regime of the quasisteady internal hydraulic theory, one of the layers becomes arrested at some point of the tidal cycle, while in

our simulations, this does not occur due to the effects of unsteadiness. In fact, simulations with longer oscillation periods show results that are closer to the quasisteady prediction of Armi and Farmer (1986) (not shown). Conditions are supercritical ($G^2 > 1$) within the channel (from cell 145 to 169 in Fig. 12a) throughout most of the tidal cycle. Maximal exchange conditions, with two control points and subcritical flow in between, only occur at two phase windows: before maximal ebb (from $4T/12$ to $5T/12$) and maximal flood (from $10T/12$ to $11T/12$). In the first of these windows, one control is located at the southern end of the channel and the other in the middle of the channel, with the latter moving southward as the tidal cycle progresses. Shortly before maximal ebb, the southern section becomes subcritical, and the only control point separates a subcritical section to the south from a supercritical section to the north. From $10T/12$ to $11T/12$, the northern control point is at the LO end of the channel, while the southernmost control is inside the channel and moves northward as the tidal cycle progresses. Only toward the end of the ebb and the flood periods, when exchange flows develop, is the flow subcritical in the channel.

During upwelling conditions (scenario 2, $F_0^2 \sim 0.5$), the velocity field still shows flow reversals at all depths at the center of the channel (Fig. 10c). However, the influence of the baroclinic forcing on the velocity field is very significant and bidirectional exchange flow occurs at the midchannel section during almost 40% of the tidal cycle at both the ebb–flood and flood–ebb transitions (Fig. 10c). Exchange flow persists longer though at the end of the ebb period. The two

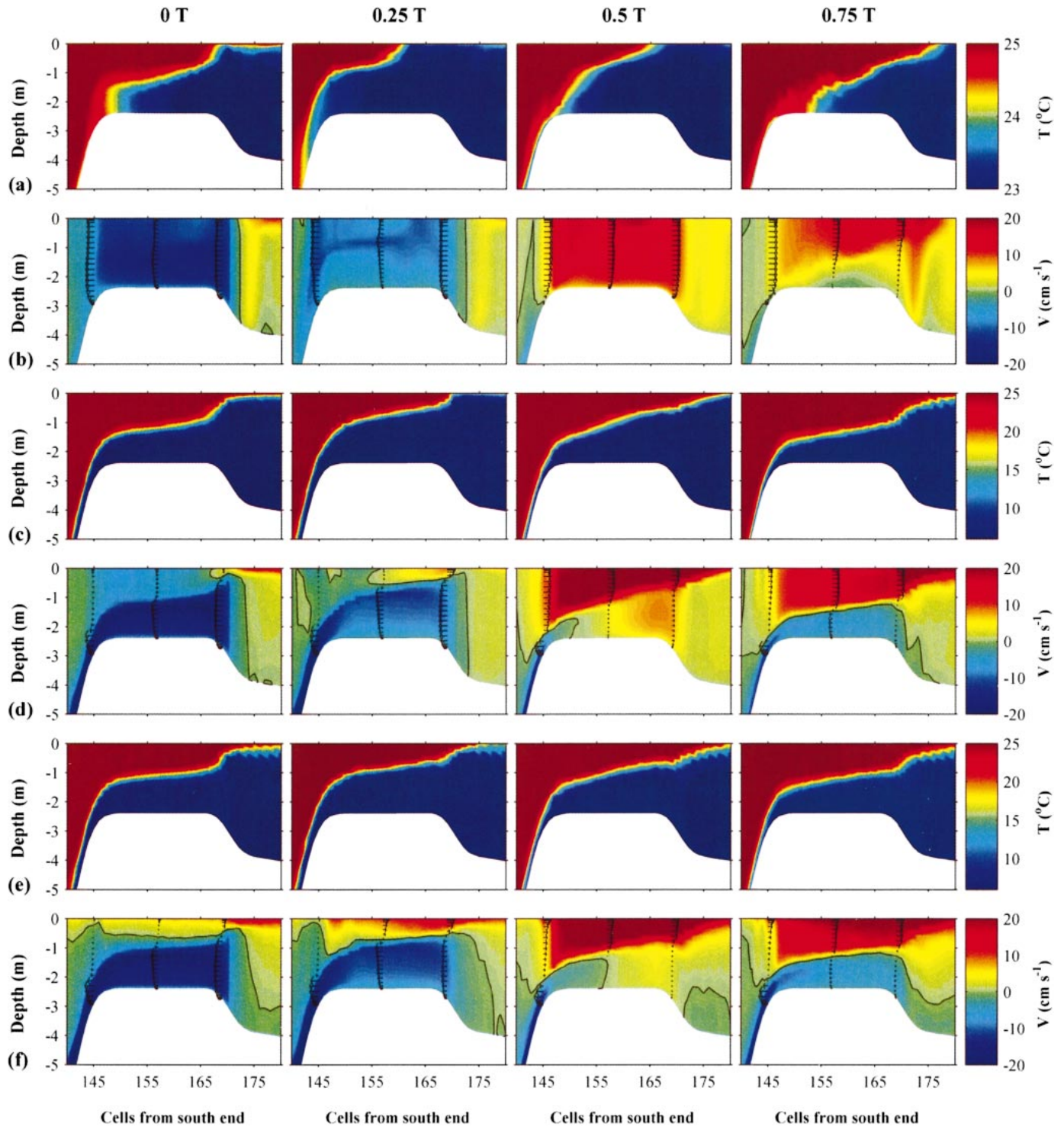


Fig. 11. Longitudinal section of temperature and velocity, for the three scenarios: scenario 1 (a–b), scenario 2 (c–d), scenario 3 (e–f).

layers are well defined in the temperature field throughout the tidal cycle (Fig. 10d) and at all points in the channel (Fig. 11c), with the interface location undergoing oscillations of up to 75 cm (Fig. 10d). The results show that one control section exists in the channel at its northern end, separating the supercritical section to the north from the subcritical section to the south during the majority of the tidal cycle (see

Fig. 12b). During flood, this control section is located at the northernmost end of the channel, and it moves southward during ebb flows. It is only at the end of the flood period ($1T/12$ to $3T/12$), when the thickness of the surface layer—as defined here—vanishes, that this control is lost. The southern end has G^2 values close to 1 but still subcritical during most of the tidal cycle, which is the result of bottom

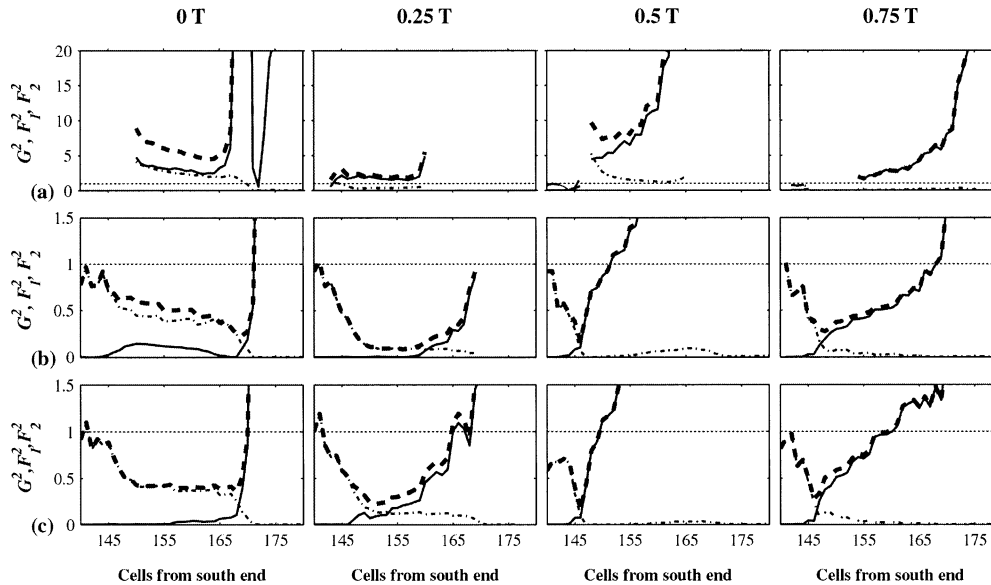


Fig. 12. Froude numbers every quarter period during a complete 2-h barotropic cycle for each of the three scenarios: (a) scenario 1, (b) scenario 2, and (c) scenario 3. The composite and layer-averaged Froude numbers are shown: G^2 (dashed line), F_1^2 (solid line), and F_2^2 (dash-dot line), along with a dotted line at Froude number equals one.

friction, as suggested by Winters and Seim (2000) for flows through smooth contractions. Only in the flood–ebb ($3T/12$ to $4T/12$) and ebb–flood ($9T/12$ to $11T/12$) transitions at the southernmost end of the channel and within LO (beyond the northern end of the channel) does the flow reach critical conditions. Hence, maximal exchange conditions occur around slack tide. The two layers are well defined throughout the tidal cycle (Fig. 11c), which might lead one to think that there is a continuous connection of LO with LSB. The longitudinal velocity profile (Fig. 11d) proves that this conclusion is incorrect and, at $T/2$ (maximum ebb), only a small wedge of water at the southern end of the channel flows toward LSB, while all other regions of the channel flow toward LO. Again, this feature is the result of unsteady effects

and might induce misinterpretations if observations were only conducted at the southern end of the channel.

Under the influence of southerly winds (scenario 3), the upper part of the water column does not experience flow reversals and always flows northward (see Figs. 10e and 11f). Bidirectional exchange flow persists in all sections of the channel during longer periods within a tidal cycle, and it is only during one fourth of the tidal cycle, around maximal ebb ($T/2$), that both layers flow northward at the northern end of the channel (Fig. 11f). Wind acts not only as a direct source of momentum for the surface layers but it also creates additional sources of mixing, increasing the mean values of K_v in scenario 3 by almost 50% with respect to scenario 2 (from 4.6×10^{-5} to $7.6 \times 10^{-5} \text{ m}^2 \text{ s}^{-1}$). The two layers remain well defined in the temperature field throughout the tidal period (Fig. 11e), with oscillations of the interface location that are smaller than in scenario 2 (Fig. 10f). The results show that two control points exist during the flood period of the tidal cycle (see Fig. 12c): one in the southern end of the channel, but already in LSB, and the other at the northern end. Subcritical flow exists between these two control points, indicating the existence of maximal exchange throughout the tidal period but not during the ebb portion of the cycle (from $5T/12$ to $9T/12$), when the southernmost control disappears. The control point existing at the northern end of the channel moves southward during ebb, with the northern end of the channel becoming supercritical. Comparing the length of time that two control sections exist in the channel (and hence maximal exchange conditions exist) for the different scenarios (Fig. 13), shows that wind pushes flow toward maximal exchange.

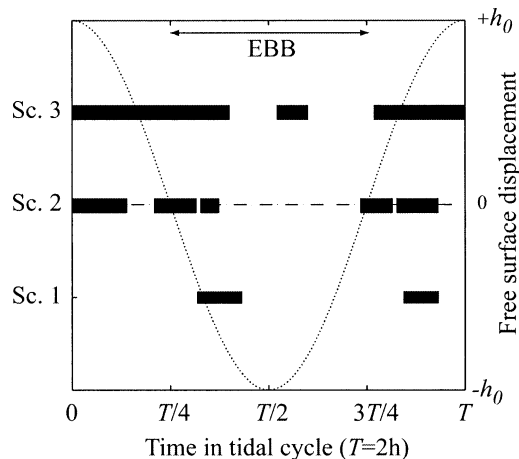


Fig. 13. Periods along a 2-h barotropic cycle in which two control points coexist (and hence maximal exchange exists) in the channel for scenarios 1–3.

Influence of the internal dynamics of LSB on exchange— Embayment stratification has been neglected in the numeri-

cal analysis of exchange processes. However, LSB is stratified during summer with top to bottom temperature differences that can reach up to 15°C in mid-August (not shown). Under these conditions, embayment upwelling events and large isotherm tilts can occur and, depending on stratification and wind speed, the internal dynamics of the embayment can influence the lake–embayment exchange processes. We use the data set collected in Experiment 4 to establish this extent. The mean temperature profile is characterized by an almost constant temperature gradient at all depths starting at ~3 m (below the mixed layer). The temperature at the bottom of the embayment is essentially constant (~12–13°C) throughout this time.

Wind over LSB across all the experiments had a strong diurnal periodicity. It was predominantly from the southwest although the most energetic events are either westerlies or northeasterlies. The wind was weak during most of the time, with mean values of 2.6 and 2.8 m s⁻¹ during Experiments 3 and 4, respectively. The relative strength of heating and wind stirring processes—competing in the generation–destruction of temperature stratification in the water column (e.g., Simpson et al. 1990)—is, on average, O(1) for Experiment 4, which explains the large and persistent vertical temperature gradients that exist in summer. On shorter time scales, of the order of individual wind events, the response of the water column to wind stress can be parameterized on the basis of the values of the Wedderburn, W , and Lake numbers, L_N (Stevens and Imberger 1996). The Wedderburn number for the nearly linear stratification observed in LSB was calculated as (Monismith 1986)

$$W = \frac{h_1 g' h_1}{L u_*^2} \quad (9)$$

with $g' = \frac{1}{2}N^2H$, $h_1 = \frac{1}{2}H$. Here, H is the depth of the basin (assumed equal to 10 m, the depth of Sta. S4), L is the basin length (here assumed to be 3400 m), $N^2 (= -g/\rho_0\partial\rho/\partial z)$ is the buoyancy frequency calculated from the top and bottom thermistors, and u_* is the wind friction velocity determined from the meteorological station measurements. The lake number is defined as

$$L_N = \frac{M_{bc}}{\tau A_s z_v} \quad (10)$$

where M_{bc} is the baroclinic moment about the center of the embayment volume, τ is the surface shear stress, A_s is the surface area, and z_v is the depth of the center of volume. In the calculation of L_N , it was assumed that the middle of the density gradient region is located 3.5 m below the diurnal mixed layer. Low lake numbers ($L_N < 1$) are associated with vertical mode 1 tilting of the temperature field, whereas low Wedderburn numbers ($W \sim O(1)$ or $W < 1$) are associated with upwind opening and downwind closing of the metalimnion, a vertical mode 2 response. High values of both numbers indicate calm conditions. Both W and L_N were calculated on a 30-min basis from data collected in Experiment 3, and are shown in Fig. 14 together with the wind records (top) and the temperature fields at Sta. S3 and S5. The magnitudes of the quarter period for the first and second mode internal waves ($T_1/4$ and $T_2/4$) are shown as horizontal bars

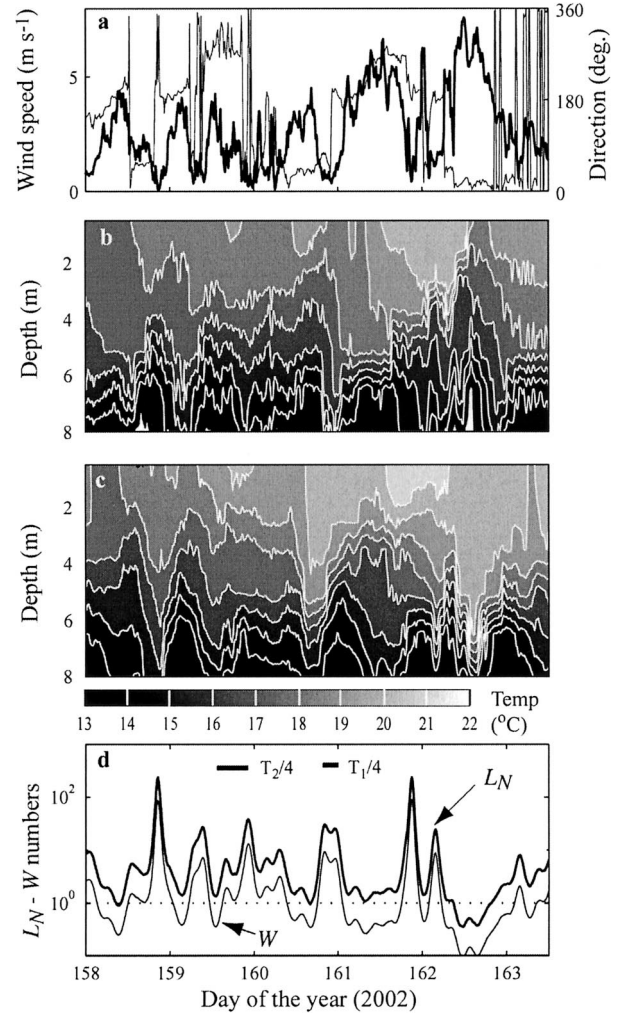


Fig. 14. Time series of (a) wind speed and direction, (b) temperatures at Sta. S3, and (c) temperature at S5 during Experiment 3. Isotherms in (b) and (c) are shown every 1°C. Panel (d) shows time series of Lake and Wedderburn numbers.

in the lower panel. These are the appropriate time scales for the minimum duration of wind events sufficient to induce tilting predicted by the Lake and Wedderburn numbers, respectively.

Figure 14 shows that the response of the basin is a combination of both vertical modes 1 and 2, as predicted by O(1) values of L_N and W during wind events. With the values of W shown in Fig. 14 ($W > 0.1$ in most cases), and using $h_1 = \frac{1}{2}H$ ($=5$ m), the time scale for the vertical entrainment to significantly change the stratification, T_* , is larger than the time scale for upwelling to occur, T_u (see Equation 18 in Stevens and Imberger 1996), with

$$\frac{T_u}{T_*} \sim W^{-3/2} \left[\frac{h_1}{L} \frac{1}{(1 - h_1/H)} \right]^{1/2} \quad (11)$$

Hence, individual wind events induce significant isotherm excursions with little entrainment. Given the strong and continuous stratification of the water column, either a mode 1 or mode 2 response will induce considerable temperature

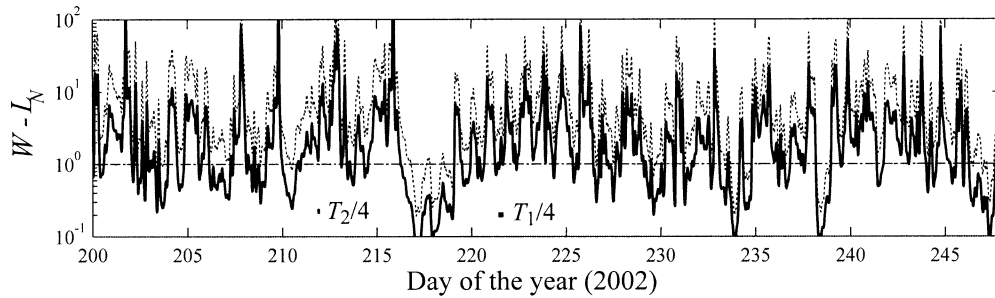


Fig. 15. Time series of Lake and Wedderburn numbers for Experiment 4.

changes at any given depth. In Sta. S3, for example, these changes are of up to 4°C at 3 m in experiment 3 (see Fig. 14). They develop in a time scale $O(T_1/4)$ and persist as long as the wind lasts. In experiment 3, $T_1/4 \sim 4\text{--}5$ h and wind persists for up to 12 h. These time scales are larger than the time scale for adjustment within the channel to changes in temperature gradients, $\tau_w \sim 1\text{--}2$ h (see above), and hence, the wind-driven internal adjustments in LSB can influence the lake–embayment exchange.

If a layered (two or three layer) model is adopted to represent the lake–embayment system, theory establishes that exchange through the channel is influenced by the conditions on either side (i.e., is submaximal) if the interface at the bottom of the surface layer in one of the reservoirs is above the interface height at the virtual control (see Armi and Farmer 1986). This occurs as long as the bottom of the epilimnion in LSB is above the bottom of the channel (i.e., less than 3 m below the free surface) and, in particular during wind-induced upwelling events at the northern end of the embayment ($L_N < 1$ in Fig. 15) when the hypolimnetic water is exposed at the surface and when second-mode displacements cause the metalimnion to reach the surface ($W < 1$ in Fig. 15) in the northern end of the embayment. These events are not uncommon in our data set and, hence, submaximal exchange is expected through the lake–embayment connection as a consequence of large isopycnal tilts in LSB.

Observations collected in LSB, a semienclosed embayment of LO, have been used to examine the transport processes responsible for the exchange of lake–embayment water masses across the lake–embayment connection (channel) and their seasonal evolution. Scaling arguments applied to the observations suggest that exchange in the channel is the result of a multiple balance in which one needs to consider spatial thermal variations (baroclinic forcing), oscillations in the water level (barotropic forcing), friction, wind stress, and unsteady effects. None of these processes is negligible in the momentum balance. Even in extreme cases, water-level oscillations are on the order of 10 cm and barotropic forcing is, hence, weak (relative to the order of magnitude stronger forcing typically seen in estuaries) but exerts a considerable influence on the channel velocity field. Temperature gradients across the channel are the result of (1) differences in thermal inertia, at the seasonal time scales, and (2) at shorter time scales (diurnal to synoptic), differences in the wind-driven internal dynamics of LSB and LO. The largest density gradients across the channel are caused by episodic upwell-

ing events in LO during the stratified season. Upwelling events can be predicted from wind and stratification, using the first-order thermocline-tilting model of Csanady (1977). The baroclinic forcing during these events controls both the exchange across the channel and internal circulation processes in the embayment.

To enhance understanding of the physical processes in the channel under more general conditions (weaker baroclinic forcing), a series of numerical experiments were conducted with the Princeton Ocean Model in LSB. These simulations showed that maximal exchange conditions (two control sections with subcritical flow in between) develop in the channel, especially around the flood–ebb or ebb–flood transitions, when baroclinic forcing is more dominant, agreeing with Armi and Farmer (1986). The details, however, do not agree with Armi and Farmer’s (1986) description of exchange flows through a contraction subject to barotropic forcing, due to the effects of unsteadiness and frictional processes. Submaximal exchange rate can result from the nonnegligible influence of friction at the bottom (see Winters and Seim 2000). Also, the influence of unsteady effects is considerable and may lead to erroneous conclusions about flow between the reservoirs if only local temperature observations are gathered. Under typical weakly stratified conditions, flow reversals occur at all depths, while at the center of the channel, there are always two layers, which might lead one to conclude that a continuous exchange flow exists, but this was shown to be incorrect. A mild along-channel wind forcing (from embayment to lake) favors the persistence of both two-layer exchange flows and maximal conditions within a tidal cycle.

In the numerical experiments, LSB is assumed to be nonstratified. Under more general conditions, with LSB stratified, the amplitude of internal oscillations in LSB and their time scales relative to the internal adjustment time scale in the channel suggest that exchange of lake and embayment waters through the channel can be subject to the influence of the embayment’s internal dynamics. Therefore, exchange across the channel can be either maximal or submaximal depending on the phasing of the internal dynamics of LSB with respect to that of LO, and wind forcing. This, together with the nonnegligible mixing between layers, makes the calculation of exchange rates challenging in LSB-like embayments. This fact precludes the possibility of getting back-of-the-envelope estimates of exchange rates and forces the researcher to use numerical simulations of circulation and exchange to properly estimate embayment–lake exchange.

References

- ANTENUCCI, J. P., J. IMBERGER, AND A. SAGGIO. 2000. Seasonal evolution of the basin-scale internal wave field in a large stratified lake. *Limnol. Oceanogr.* **45**: 1621–1638.
- ARMI, L., AND D. M. FARMER. 1986. Maximal two-layer exchange through a contraction with barotropic net flow. *J. Fluid Mech.* **164**: 27–51.
- ASSAF, G., AND A. HECHT. 1974. Sea straits: A dynamical model. *Deep-Sea Res.* **21**: 947–958.
- BLUMBERG, A. F., AND G. L. MELLOR. 1987. A description of a three-dimensional coastal ocean circulation model, p. 1–16. *In* N. S. Heaps [ed.], Three dimensional coastal ocean models. American Geophysical Union.
- BURLING, M. C., G. N. IVEY, AND C. B. PATTIARATCHI. 1999. Convectively driven exchange in a shallow coastal embayment. *Continental Shelf Res.* **19**: 1599–1616.
- COWEN, E. A., I. M. SOU, P. L.-F. LIU, AND B. RAUBENHEIMER. 2003. PIV measurements within a laboratory generated swash zone. *J. Eng. Mech.* **129**: 1119–1129.
- CSANADY, G. T. 1977. Intermittent 'full' upwelling in Lake Ontario. *J. Geophys. Res.* **82**: 397–419.
- FARMER, D. M., AND L. ARMI. 1986. Maximal two-layer exchange over a sill and through the combination of a sill and a contraction with barotropic flow. *J. Fluid Mech.* **164**: 53–76.
- FINNIGAN, T. D., AND G. N. IVEY. 1999. Submaximal exchange between a convectively forced basin and a large reservoir. *J. Fluid Mech.* **378**: 357–378.
- , AND ———. 2000. Convectively driven exchange in a stratified sill-enclosed basin. *J. Fluid Mech.* **418**: 313–338.
- FINNIGAN, T. D., K. B. WINTERS, AND G. N. IVEY. 2001. Response characteristics of a buoyancy-driven sea. *J. Phys. Oceanogr.* **31**: 2721–2736.
- FUSSMAN, G. F., S. P. ELLNER, K. W. SHERTZER, AND N. G. HAIRSTON. 2000. Crossing the Hopf Bifurcation in a live predator–prey system. *Science* **290**: 1358–1360.
- GREGG, M. C. 2004. Small-scale processes in straits. *Deep Sea Res. II* **51**: 489–503.
- HAMBLIN, P. F. 1982. On the free surface oscillations of Lake Ontario. *Limnol. Oceanogr.* **27**: 1039–1049.
- HELFRICH, K. R. 1995. Time-dependent two-layer hydraulic exchange flows. *J. Phys. Oceanogr.* **25**: 359–373.
- IMBERGER, J., AND G. IVEY. 1991. On the nature of turbulence in a stratified fluid. Part II: Observations. *J. Phys. Oceanogr.* **21**: 659–680.
- IVEY, G. N. 2004. Stratification and mixing in sea straits. *Deep Sea Res. II* **51**: 441–453.
- , AND J. IMBERGER. 1991. On the nature of turbulence in a stratified fluid. Part I: The energetics of mixing. *J. Phys. Oceanogr.* **21**: 650–658.
- LUKETINA, D. A., AND J. IMBERGER. 1989. Turbulence and entrainment in a buoyant surface plume. *J. Geophys. Res.* **94**(C9): 12619–12636.
- MONISMITH, S. G. 1986. An experimental study of the upwelling response of stratified reservoirs to surface shear stress. *J. Fluid Mech.* **171**: 407–439.
- MONSEN, N. E., J. E. CLOERN, L. V. LUCAS, AND S. G. MONISMITH. 2002. A comment on the use of flushing time, residence time, and age as transport time scales. *Limnol. Oceanogr.* **47**: 1545–1553.
- OFFICER, C. B. 1976. *Physical Oceanography of Estuaries*. Wiley.
- RUEDA, F. J., S. G. SCHLADOW, AND S. O. PALMARSSON. 2003. Basin-scale internal wave dynamics during a winter cooling period in a large lake. *J. Geophys. Res.* **108**: [doi: 10.1029/2001JC000942]
- SCHWAB, D. J. 1977. Internal free oscillations in Lake Ontario. *Limnol. Oceanogr.* **22**: 700–708.
- SHAW, W. J., AND J. H. TROWBRIDGE. 2001. The direct estimation of near-bottom turbulent fluxes in the presence of energetic wave motions. *J. Atmospher. Ocean. Technol.* **18**: 1540–1557.
- SIMPSON, J. H., J. BROWN, J. MATTHEWS, AND G. ALLEN. 1990. Tidal straining, density currents, and stirring in the control of estuarine stratification. *Estuaries* **13**: 125–132.
- STEVENS, C., AND J. IMBERGER. 1996. The initial response of a stratified lake to a surface shear stress. *J. Fluid Mech.* **312**: 39–66.
- WINTERS, K. B., AND H. E. SEIM. 2000. The role of dissipation and mixing in exchange flow through a contracting channel. *J. Fluid Mech.* **407**: 265–290.

Received: 20 January 2004

Accepted: 11 July 2004

Amended: 13 September 2004